Geologia USP
Série Científica

Revista do Instituto de Geociências - USP
Geol. USP, Sér. cient., São Paulo, v. 10, n. 3, p. 97-117, outubro 2010

Tourmaline and Rutile as Indicators of a Magmatic-hydrothermal Origin for Tourmalinite Layers in the São José do Barreiro Area, NE Ribeira Belt, Southern Brazil

Turmalina e Rutilo como Indicadores da Origem Magmática-hidrotermal dos Níveis de Turmalinito de São José do Barreiro, Cinturão Ribeira, Sudeste do Brasil

Gianna Maria Garda[1] (giagarda@usp.br), Paulo Beljavskis[1] (beljavskis@terra.com.br),
Liz Zanchetta D'Agostino[2] (lizanca@gmail.com), Michael Wiedenbeck[3] (michawi@gfz-potsdam.de)
[1]Departamento de Mineralogia e Geotectônica - Instituto de Geociências - USP
R. do Lago 562, CEP 05508-080, São Paulo, SP, BR
[2]Laboratório de Caracterização Tecnológica - POLI/USP, São Paulo, SP, BR
[3]Helmholtz Centre Potsdam - GFZ German Research Centre for Geosciences, Potsdam, DE

Received 04 May 2010; accepted 04 August 2010

ABSTRACT

Tourmalines from tourmaline-rich layers intercalated with schists of the Rio Una Unit of the Embu Complex and from coarse-grained tourmalinite layers associated with quartzite from São José do Barreiro and Formoso (Central Ribeira Belt, São Paulo State, Brazil) were analyzed for major, trace- and rare-earth elements and boron stable isotopes. Two main phases of tourmaline formation were identified by mineral chemistry. The tourmalines from the schist-hosted tourmaline layers are characterized by relatively low MgO (from 4.7 to 6.5%), Na_2O (1.5 to 2.1%) and CaO (from 0.2 to 1.1%) contents and high Al_2O_3 (from 32 to 35%) and FeO (from 6.7 to 9.0%) contents, and also by two $(REE)_{CN}$ patterns, one represented by $(La/Yb)_{CN}$ from 2.7 to 4.3 and positive Eu anomalies, and the other by $(La/Yb)_{CN}$ from 0.2 to 0.3 and practically no Eu anomaly. The variations in major-element contents reflect the composition of the rock being metamorphosed and in which tourmaline is crystallizing, whereas the $(REE)_{CN}$ patterns indicate the evolution of the metamorphic fluid in face of changing metamorphic conditions. The tourmaline of the tourmalinite layers intercalated in quartzite is characterized by relatively high Al_2O_3 (from 32.3 to 33.92%), FeO (from 6.54 to 7.3%) and Na_2O (from 1.8 to 2.1%) contents and very low total REE (3.5 ppm) contents, in particular of HREE. The $(REE)_{CN}$ pattern for this tourmaline is characterized by a positive Eu anomaly, indicating a high fluid/rock ratio. The $\delta^{11}B$ values for this tourmaline fall in the -12.3 and -13.9‰ interval. On the other hand, the tourmaline of a massive tourmalinite also associated with quartzite has the highest MgO (from 7.3 to 9.7%), CaO (from 0.8 to 2.5%), F, Th, U, Hf, Zr, Y, Sr and total REE (305 ppm) contents and the lowest Al_2O_3 (from 28.6 to 31.8%) and FeO (from 5.4 to 8.3%) contents, when compared to the other tourmalines analyzed. Differing from all other $(REE)_{CN}$ patterns, the one that characterizes this tourmaline is LREE-enriched [$(La/Yb)_{CN}$ = 5.8] and shows a slightly negative Eu anomaly. Negative $\delta^{11}B$ values in the -13.9 and -15.8‰ interval indicate, as the other interval, filiation with S-type granite magmatism-hydrothermalism. The massive tourmalinite also contains zircon, scheelite, and monazite as accessory minerals and relatively abundant (green and red) rutile. The green rutile is enriched in Nb, Al, Fe and Sn when compared to the red rutile, which is Cr rich. The differences in composition observed in the tourmaline and rutile of the massive tourmalinite indicate the involvement of magmatic-hydrothermal fluids with metamorphic fluids from which tourmaline and other minerals crystallized. The syn-collisional, S-type São José do Barreiro Granite is the possible source for the magmatic-hydrothermal fluids.

Keywords: Tourmalinites; Rutile; São José do Barreiro Granite; REE in tourmaline.

RESUMO

Turmalinas de níveis ricos em turmalina intercalados com os xistos da Unidade Rio Una do Complexo Embu e de turmalinitos grossos associados a quartzito da região de São José do Barreiro e Formoso (Cinturão Ribeira, SP, Brasil) foram analisadas para elementos maiores, traço e terras raras e isótopos estáveis de boro. Duas fases principais de formação de

turmalina foram identificadas pela química mineral. A primeira fase, que corresponde a níveis ricos em turmalina intercalados em xistos, caracteriza-se pelos teores relativamente baixos de MgO (entre 4,7 e 6,5%), Na_2O (1,5 e 2,1%) e CaO (entre 0,2 e 1,1%) e altos de Al_2O_3 (entre 32 e 35%) e FeO (entre 6,7 e 9,0%). Dois padrões de elementos terras raras (normalizados para o condrito C1) são representados respectivamente por razões $(La/Yb)_{NC}$ de 2,7 a 4,3 e anomalias positivas de Eu e razões $(La/Yb)_{NC}$ de 0,2 a 0,3 e anomalias de Eu praticamente ausentes. As variações nos teores de elementos maiores refletem as composições da rocha hospedeira que está sendo metamorfizada e na qual a turmalina está se cristalizando, ao passo que os padrões de ETR indicam a evolução do fluido metamórfico face às condições de metamorfismo. A segunda fase de turmalina, que compõe níveis de turmalinito intercalados com quartzito, caracteriza-se pelos teores relativamente elevados de Al_2O_3 (entre 32,3 e 33,92%), FeO (entre 6,54 e 7,3%) e Na_2O (entre 1,8 e 2,1%) e teores muito baixos de ERT total (3,5 ppm), em particular de ETR leves. O padrão de ETR para esta turmalina caracteriza-se pela anomalia positiva de Eu, o que indica alta razão fluido/rocha. Os valores de $\delta^{11}B$ obtidos para esta turmalina caem no intervalo entre -12,3 e -13,9‰. No extremo oposto, a turmalina do turmalinito maciço, também associado a quartzito, apresenta os teores mais altos de MgO (entre 7,3 e 9,7%), CaO (entre 0,8 e 2,5%), F, Th, U, Hf, Zr, Y, Sr e ETR total (305 ppm) e os mais baixos de Al_2O_3 (entre 28,6 e 31,8%) e FeO (entre 5,4 e 8,3%), quando comparada às demais turmalinas analisadas. Diferentemente dos demais padrões de ETR, o que caracteriza esta turmalina é o enriquecimento em ETR leves [$(La/Yb)_{NC}$ = 5,8] e leve anomalia negativa de Eu. Valores negativos de $\delta^{11}B$ no intervalo entre -13.9 e -15.8‰ indicam, tal qual o anterior, a filiação com magmatismo-hidrotermalismo granítico do tipo S. O turmalinito maciço também contém zircão, scheelita e monazita como minerais acessórios e rutilo (verde e vermelho) abundante. O rutilo verde é mais enriquecido em Nb, Al, Fe e Sn do que o rutilo vermelho que, por sua vez, é mais rico em Cr. As diferenças nas composições da turmalina e do rutilo do turmalinito maciço indicam o envolvimento de fluidos magmáticos-hidrotermais na evolução dos fluidos metamórficos dos quais turmalina e outros minerais cristalizaram-se. O Granito São José do Barreiro, do tipo S e sin-colisional, é a possível fonte desses fluidos magmáticos-hidrotermais.

Palavras-chave: Turmalinito; Rutilo; Granito São José do Barreiro; ETR em turmalina.

INTRODUCTION

São José do Barreiro and Formoso are located in the central part of the Neoproterozoic Ribeira Belt, about 260 km east of São Paulo city. In that hilly area, tourmaline-rich layers, which are usually associated with quartzite, are known as *saibreiras* (UFRJ/CPRM, 2007) and stand out in relief from the surrounding rocks.

Pereira, Ávila and Moura (2001) described tourmaline-rich boudins and layers in the region limited by Campos de Cunha, Areias and Formoso, which are hosted by schists of the Rio Una Unit of the Embu Complex (Figure 1). These authors also used the occurrence of tourmaline-rich layers to distinguish the Rio Una Unit quartzites from those of the Redenção da Serra Unit (also Embu Complex). In a following exploratory study on the tin potentiality of the Funil and São José do Barreiro granitic bodies, Pereira, Ávila and Neumann (2003) observed a constant association of cassiterite with coarse-grained black tourmaline and quartz in pan mineral concentrates. The coarse-grained tourmaline was genetically related to pegmatitic bodies and to quartz-tourmaline veins. Another type of tourmaline, finer-grained and light brown, was related to the tourmalinite layers that frequently occur in the study area.

Tourmaline is considered a recorder of petrogenetic information (e.g., Henry and Guidotti, 1985; Jolliff, Papike, Laul, 1987; Palmer and Slack, 1989; Slack, 1996; Marchall and Ludwig, 2006; Bortnikov et al., 2008) because it can accommodate a large variety of cations in terms of size and charge in its structure and as a consequence it acquires the geochemical signature of the medium from which it crystallized.

In the *saibreiras* we also found rutile in considerable quantities. In recent years rutile chemistry and thermometry have been used as a guide to provenance for a variety of geological settings (e.g., Zack, Von Eynatten, Kronz, 2004; Zack, Moraes, Kronz, 2004; Fernández, Schalamuk, Omenetto, 2005; Müller and Halls, 2005; Meinhold et al., 2008; Morton and Chenery, 2009), because rutile is chemically and physically stable and not prone to destruction during the sedimentation cycle.

In order to further investigate the possible genetic relationships between schist-hosted tourmaline-rich layers and the tourmalinite layers in the *saibreiras* of the São José do Barreiro-Formoso area, a geochemical study was carried out, including major-element, trace-element and boron stable isotope analyses of tourmaline and rutile chemistry.

GEOLOGIC SETTING

The Ribeira Belt extends for more than 1,400 km along the southeastern coast of Brazil and is the main tectonic unit of the Mantiqueira Province (Hasui and Oliveira, 1984). It resulted from the collision of the São Francisco, Congo and Rio de la Plata cratons during the agglutination of Western Gondwana in the Brasiliano event (e.g., Roig,

Dantas, Menezes, 2004). The study area is located in the Embu domain of the central Ribeira Belt, delimited from surrounding domains by dextral transcurrent faults (Cubatão and Alto da Fartura Shear Zones), and is partially covered by the Tertiary Resende and Taubaté basins (Figure 1).

The Embu Domain is made up of the metasedimentary rocks of the Embu Complex. The Rio Una and the Redenção da Serra units of the Embu Complex are recognized in the study area (Pereira, Ávila, Moura, 2001). The Rio Una Unit is composed of fine- to medium-grained (quartz-muscovite, biotite-muscovite, sillimanite and quartzo-feldspatic) schists, which are intercalated with quartzite, tourmalinite layers and amphibolitic rocks. The Rio Una Unit is in direct contact with the migmatites and garnet-biotite gneisses of the Redenção da Serra Unit to NW and with a number of granites and granitoids of Mesoproterozoic to Cambrian ages (Figure 1).

Pereira, Moura and Bustamante-Junho (2002) identified five magmatic episodes in the central portion of the Ribeira Belt: pre-collisional (630 - 595 Ma), syn-collisional 1 (605 - 565 Ma), syn-collisional 2 (565 - 540 Ma), late-collisional (540 - 520 Ma) and post-collisional (520 - 480 Ma). The undeformed Funil Granite (50 km^2) crops out northwest of São José do Barreiro and is composed of leucocratic, gray to pinkish, porphyritic and fine-grained

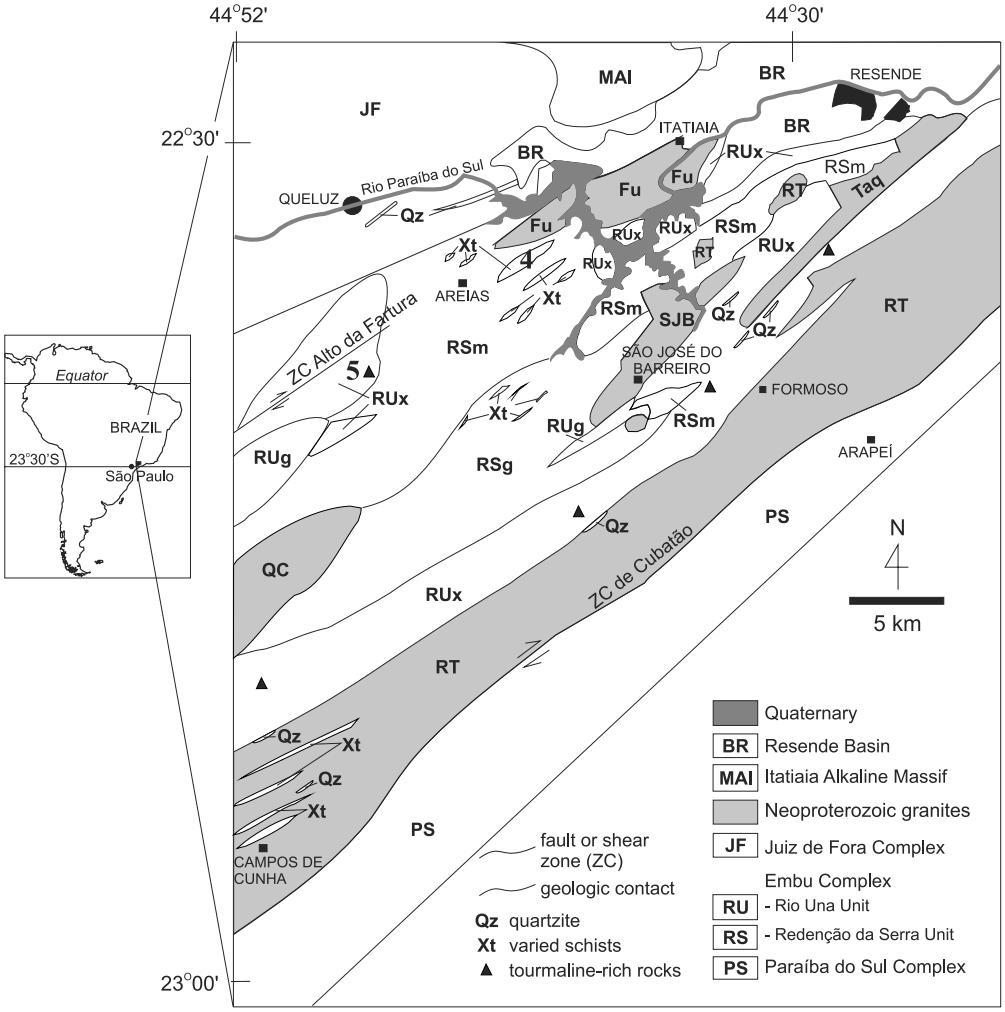

Figure 1. Simplified geologic map of the Queluz-Resende-Campos de Cunha region (mod. after Pereira, Ávila, Moura, 2001). Neoproterozoic granites: **RT** = Rio Turvo (579 ± 6 Ma); **SJB** = São José do Barreiro (603 ± 3 Ma); **QC** = Quebra-Cangalha; **Fu** = Funil (584 ± 5 Ma); **Taq** = Taquaral (605 ± 11 Ma). Embu Complex, Redenção da Serra Unit: **RSg** = biotite-garnet gneisses; **RSm** = migmatites, augen gneisses, banded gneisses, quartzites; Rio Una Unit: **RUx** = varied schists with quartzite and tourmalinite intercalations; **RUg** = fine biotite gneisses. Points 1, 2, 4, 5 and 8 correspond to tourmalinite layers of the Rio Una Unit sampled by R. M. Pereira and referred to in the text as SRJ.

equigranular rocks of I-type compositional affinity (Pereira, Moura, Bustamante-Junho, 2002; Pereira, Ávila, Neumann, 2003). The foliated São José do Barreiro Granite (45 km^2) is a dark-gray, medium-grained, inequigranular to porphyritic biotite granite characterized as S-type and showing a strong REE fractionation. Both granites are related to the syn-collisional 1 episode of Pereira, Moura and Bustamante-Junho (2002): the São José do Barreiro Granite (603 ± 3 Ma) formed prior to the regional metamorphism, whereas the Funil Granite (584 ± 5 Ma) is coeval with the metamorphic peak (579 Ma).

TOURMALINES

Materials and methods

Five samples of tourmaline separates corresponding to the Rio Una Unit schist-hosted tourmaline-rich layers (Figure 1) were kindly donated for this study by Dr. Ronaldo Mello Pereira (Universidade do Estado do Rio de Janeiro). The crystals were mounted in epoxy resin and polished for microprobe analysis. The five samples are referred to in the text as SRJ-01, SRJ-02, SRJ-04, SRJ-05 and SRJ-08.

In addition to the tourmaline separates, whole-rock samples from a schist-hosted tourmaline-rich layer and tourmalinites intercalated in *saibreira* were also analyzed. Sample BM2 was collected close to point 8 in Figure 1 and is from a garnet-biotite schist containing color-zoned, poikiloblastic tourmaline (Figure 2A). Samples SJB-3A and SBJ-3B were collected close to the Camponesa Farm, 5 km east of São José do Barreiro (point 2 of Figure 1). Sample SJB-3A is from a thin tourmalinite layer intercalated in quartzite (*saibreira*) and is composed of color-zoned tourmaline (Figure 2B). Sample SJB-3B is from a massive tourmalinite formed by coarse-grained, irregularly zoned tourmaline (Figure 2C). Rutile is also abundant in this sample and will be further analyzed in more detail. Polished thin sections of samples BM2, SJB-3A and SJB-3B were prepared for electron microprobe and secondary ion mass spectrometry analyses.

The five SRJ samples and tourmaline separates from SJB-3A and SJB-3B were analyzed by inductively-coupled plasma mass spectrometry for trace-element and REE concentrations.

The polished thin sections and epoxy mounts of the SRJ tourmaline separates were coated with carbon for the electron microprobe analysis (EMPA). The WDS analyses of tourmaline were performed with the JEOL Superprobe JXA-8600 at the Microprobe Laboratory of the *Instituto de Geociências* (São Paulo University). Operating conditions were: beam diameter 1 - 2 μm, beam current 15 nA and

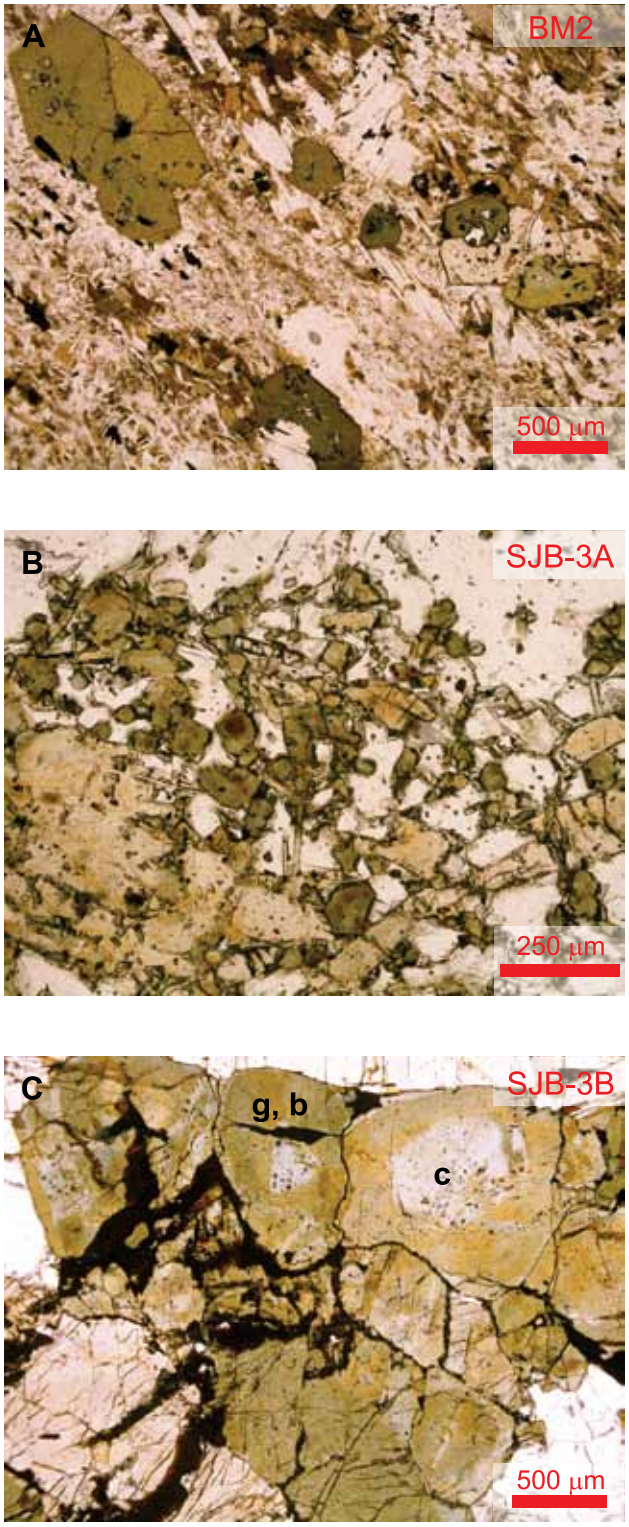

Figure 2. Photomicrographs (plane-polarized light) of colored-zoned tourmalines from samples BM2, SJB-3A and SJB-3B. Gray (c), green (g) and brown (b) zones are signaled on a SJB-3B tourmaline crystal.

acceleration voltage 15 kV. Standards, element lines and counting times were: wollastonite (Si Kα): 5 - 20 s; rutile (Ti Kα): 10 - 30 s; hornblende: (Al Kα): 10 - 20 s; olivine (Fe Kα): 5 - 20 s; Cr_2O_3 (Cr Kα): 50 s; olivine (Mn Kα) 20 - 30 s; diopside (Mg Kα): 20 - 30 s; wollastonite (Ca Kα): 10 s; albite (Na Kα1): 5 - 20 s; microcline (K Kα): 10 s; apatite A408 (F Kα): 10 s; chloroapatite CLAP (Cl Kα): 10 s.

The inductively-coupled plasma mass spectrometry (ICP-MS) analyses of the five SRJ and SJB-3A and SJB-3B tourmaline separates were conducted on sample solutions at the Chemistry Laboratory of *Instituto de Geociências* (São Paulo University) equipped with a Perkin Elmer ELAN 6100 DRC mass spectrometer, using a routine adapted from Navarro (2004). Besides REE, Rb, Sr, Y, Zr, Nb, Cs, Ba, Hf, Pb, Th and U were analyzed.

The boron isotopic composition of tourmaline was determined with a Cameca ims-6f instrument at GeoForschungZentrum in Potsdam (Germany) using methods described in detail by Garda et al. (2009). This study was part of the project: "*Isotopia do boro em turmalinitos e rochas ricas em turmalina e veios de quartzo do Anticlinal de Mariana (Minas Gerais) e Cinturão Ribeira (São Paulo), SE do Brasil*", financed by FAPESP (Proc. 2007/53895-4). The polished thin sections of samples SJB-3A and SJB-3B used for microprobe analysis were prepared for secondary ion mass spectrometry (SIMS) analyses by light polishing with 1 micron alumina and distilled water to remove the carbon, then cleaning in an ultrasonic ethanol bath and coating with a ~35 nm-thick high-purity gold layer. SIMS analyses employed a primary $^{16}O^-$ beam at nominal 12.5 kV and 0.8 nA focused to about 15 μm diameter on the sample surface. Instrumental mass fractionation (IMF) and analytical quality were determined by means of the tourmaline reference materials dravite (HS #108796), elbaite (HS #98144) and schorl (HS #112566) from the Harvard Mineralogical Museum (Dyar et al., 2001), resulting in an external repeatability of 1.7‰ (1σ). The corrected $^{11}B/^{10}B$ ratios are expressed in the standard delta notation relative to NIST SRM-951 using the value $^{11}B/^{10}B = 4.04362$ (Catanzaro et al., 1970).

Chemical composition of tourmalines

Major elements by EMPA

Tourmalines from samples SRJ mounted in epoxy resin and BM2, SJB-3A and SJB-3B polished thin sections were analyzed for major elements and F. As shown in Table 1, Cr_2O_3 and Cl were also analyzed, resulting in average 0.03 wt.% Cr_2O_3 and 0.004 wt.% Cl contents, which are close to the electron microprobe detection limits and therefore negligible.

In Figures 3 and 4 the chemical compositions of tourmaline are represented separately for the collection of samples labelled SRJ and for BM2, SJB-3A and SJB-3B. For comparison, the fields defined by SRJ tourmaline compositions are represented in both figures.

Figure 3A reproduces Henry and Guidotti (1985) Al-Fe-Mg diagram and shows that SRJ-01, SRJ-04, SRJ-05 and SRJ-08 plot in field 4 (metapelites and metapsammites coexisting with an Al-saturating phase), which is in agreement with the whole-rock composition of the Rio Una Unit schists. On the other hand, SRJ-02 plots in field 5 (metapelites and metapsammites not coexisting with an Al-saturating phase).

Although all SRJ tourmaline compositions fall intermediate to the schorl-dravite series, differences in composition are observed when major element contents are plotted against Mg# [Mg# = Mg/(Mg+Fe), atomic proportions]. Sample SRJ-02 (average Mg# = 0.70) differs from the other SRJ tourmalines (0.49 < average Mg# < 0.61) by virtue of its higher SiO_2 and Na_2O contents and lower Al_2O_3 and FeO contents (Table 1 and Figure 4).

The BM2 tourmalines (average Mg# = 0.59) plot in the fields defined by SRJ-01, SRJ-04, SRJ-05 and SRJ-08 both in Figures 3 and 4, but relative to those, BM-2 has lower SiO_2 and higher Al_2O_3 and FeO contents. Samples SJB-3A (average Mg# = 0.64) and SJB-3B (average Mg# = 0.72) plot close to the fields defined by SRJ-02. Part of SJB-3B analyses plot in field 5 of Henry and Guidotti (1985) diagram (Figure 3B) and another part in field 6 (Fe^{3+}-rich quartz-tourmaline rocks, calc-silicate rocks, and metapelites).

Compositional variations in SJB-3B tourmalines are much wider than for the other samples (MgO: 7.5 - 10 wt.%; Al_2O_3: 28.5 - 32.8 wt.%; FeO: 5.1 - 6.0 wt.%; CaO: 0.5-3 wt.%, and Na_2O: 1.3 - 2.4 wt.%), some of the compositions tending to the Ca-rich end-member uvite $[Ca(Mg,Fe^{2+})_3MgAl_5(OH)F(BO_3)_3Si_6O_{18}]$. In these cases, F contents are higher, reaching 0.3 wt.% (Figure 4L). These wide compositional variations also occur within a single crystal. In Figures 3B and 4G to 4L the compositions corresponding to green (g), gray (c) and brown (b) zones of an SJB-3B tourmaline crystal (Figure 2) are represented with black triangles. Al_2O_3, MgO and CaO contents are higher at the gray zone (c), whereas FeO, TiO_2, and Na_2O contents are higher at the green (g) and brown (b) zones.

The EMPA results characterize tourmalines according to major-element compositions as follows:

1. tourmaline from schist-hosted tourmaline-rich layers (SRJ-01, SRJ-04, SRJ-05, SRJ-08 and BM2), with Mg# < 0.65 and higher Al_2O_3 and FeO contents, lower Na_2O contents and slightly lower CaO contents. The SRJ-02

Table 1. Chemical compositions (wt.%) of tourmaline from the Rio Una Unit schists (SRJ and BM2) and São José do Barreiro tourmalinite layers (SJB-3A and SJB-3B). Ions calculated on the basis of 29 oxygen atoms and 3 boron atoms. **n.d.** = not determined.

Sample	BM													
	2-1	2-2	2-3	2-4a	2-4b	2-5	2-6	2-7	2-14	2-15	2-16	2-17	2-18a	2-18b
SiO_2	35.66	35.81	36.10	35.87	35.67	36.34	33.67	35.05	34.72	35.30	35.94	35.65	35.07	36.52
TiO_2	0.71	0.31	0.62	0.46	0.83	0.42	0.60	0.57	0.64	0.73	0.51	0.39	0.58	0.63
Al_2O_3	34.51	35.22	34.50	34.84	34.12	34.78	34.84	34.47	34.86	34.41	34.24	34.46	34.64	35.56
Cr_2O_3	0.05	0.07	0.03	0.08	0.06	0.03	0.06	0.08	0.03	0.05	0.05	0.04	0.01	0.06
FeO	7.29	7.28	7.38	7.48	7.49	7.43	6.99	6.75	7.09	7.30	7.01	7.13	7.06	6.16
MnO	0.00	0.01	0.01	0.02	0.04	0.00	0.04	0.04	0.03	0.03	0.02	0.05	0.01	0.01
MgO	5.78	5.56	5.96	5.60	5.80	5.54	5.69	6.12	5.75	5.93	6.01	6.21	6.04	4.99
CaO	0.85	0.68	0.83	0.62	0.64	0.65	1.04	0.97	1.14	0.79	1.05	1.05	0.92	0.81
Na_2O	1.79	1.64	1.76	1.79	1.82	1.61	1.67	1.78	1.67	1.75	1.64	1.73	1.76	1.60
K_2O	0.02	0.00	0.00	0.00	0.00	0.01	0.02	0.00	0.00	0.01	0.01	0.01	0.01	0.27
F	0.045	0.173	0.085	0.056	0.07	0.06	0.004	0.156	0.245	0.059	0.101	0.144	0.043	0.056
Cl	0.004	n.d.	n.d.	n.d.	n.d.	n.d.	n.d.	0.003	n.d.	n.d.	n.d.	0.001	n.d.	n.d.
SiT	5.780	5.764	5.804	5.799	5.795	5.860	5.609	5.704	5.634	5.747	5.813	5.751	5.722	5.868
AlT	0.220	0.236	0.196	0.201	0.205	0.140	0.391	0.296	0.366	0.253	0.187	0.249	0.278	0.132
AlZ	6.000	6.000	6.000	6.000	6.000	6.000	6.000	6.000	6.000	6.000	6.000	6.000	6.000	6.000
AlY	0.376	0.445	0.344	0.441	0.330	0.471	0.450	0.317	0.304	0.351	0.344	0.307	0.384	0.602
SiY	0.000	0.000	0.000	0.000	0.000	0.000	0.000	0.000	0.000	0.000	0.000	0.000	0.000	0.000
Ti	0.087	0.037	0.075	0.056	0.101	0.050	0.075	0.070	0.078	0.089	0.062	0.048	0.071	0.076
Mg	1.396	1.333	1.429	1.349	1.405	1.331	1.412	1.484	1.391	1.438	1.449	1.493	1.469	1.195
Cr	0.007	0.009	0.003	0.010	0.007	0.004	0.007	0.010	0.004	0.006	0.007	0.005	0.001	0.008
Fe3	0.000	0.000	0.000	0.000	0.000	0.000	0.000	0.000	0.000	0.000	0.000	0.000	0.000	0.000
Fe2	0.988	0.980	0.992	1.011	1.017	1.001	0.974	0.919	0.963	0.993	0.948	0.962	0.963	0.828
Mn	0.000	0.002	0.001	0.003	0.006	0.000	0.006	0.005	0.005	0.004	0.003	0.007	0.002	0.001
Ca	0.147	0.118	0.143	0.107	0.112	0.113	0.185	0.169	0.198	0.138	0.181	0.182	0.160	0.139
Na	0.561	0.511	0.548	0.560	0.572	0.503	0.538	0.562	0.527	0.553	0.516	0.541	0.557	0.497
K	0.004	0.001	0.000	0.000	0.000	0.001	0.004	0.000	0.000	0.001	0.003	0.002	0.001	0.055
Mg#	0.59	0.58	0.59	0.57	0.58	0.57	0.59	0.62	0.59	0.59	0.60	0.61	0.60	0.59

(cont.)

Table 1. (continued)

Sample	BM			SBJ										
	2-19a	2-19b	2-20	3A-1	3A-2	3A-3	3A-4	3A-5	3A-6	3A-7	3A-8	3A-9a	3A-9b	3B-1-1
SiO_2	35.88	35.13	35.49	36.36	36.60	36.43	35.84	36.72	36.58	35.23	36.39	36.83	37.16	36.92
TiO_2	0.29	0.60	0.75	0.16	0.17	1.47	0.19	0.76	0.53	0.76	0.49	0.41	0.56	0.66
Al_2O_3	35.10	34.81	35.00	33.58	33.19	31.09	33.48	32.87	33.10	33.20	32.92	33.40	34.26	31.11
Cr_2O_3	0.03	0.04	0.05	0.03	0.02	0.00	0.00	0.02	0.03	0.03	0.02	0.00	0.05	0.02
FeO	6.86	6.99	7.17	7.41	6.67	7.62	6.74	7.04	6.33	6.96	6.98	6.62	6.83	5.82
MnO	0.02	0.03	0.00	0.09	0.09	0.09	0.05	0.06	0.06	0.07	0.07	0.05	0.09	0.07
MgO	5.92	5.62	5.86	5.87	6.87	6.88	6.50	6.90	7.24	6.95	7.08	7.13	6.83	8.71
CaO	0.97	0.75	1.02	0.24	0.42	1.13	0.36	0.94	0.76	0.74	0.69	0.70	0.84	1.24
Na_2O	1.66	1.78	1.75	2.00	2.22	1.82	2.08	1.90	2.16	2.06	2.06	2.01	1.83	2.07
K_2O	0.01	0.01	0.01	0.01	0.01	0.00	0.02	0.02	0.00	0.00	0.00	0.02	0.00	0.01
F	0.015	0.06	0.1	0.043	0.057	0.06	0.089	0.085	0.057	0.073	0.088	0.111	0.097	0.058
Cl	n.d.	n.d.	0.005	n.d.	0.003	n.d.	n.d.	n.d.	n.d.	n.d.	n.d.	0.004	n.d	0.001
SiT	5.797	5.740	5.710	5.943	5.936	5.946	5.874	5.905	5.899	5.761	5.884	5.898	5.871	5.970
AlT	0.203	0.260	0.290	0.057	0.064	0.054	0.126	0.095	0.101	0.239	0.116	0.102	0.129	0.030
AlZ	6.000	6.000	6.000	6.000	6.000	5.929	6.000	6.000	6.000	6.000	6.000	6.000	6.000	5.903
AlY	0.482	0.445	0.348	0.415	0.281	0.000	0.342	0.138	0.192	0.162	0.160	0.204	0.252	0.000
SiY	0.000	0.000	0.000	0.000	0.000	0.000	0.000	0.000	0.000	0.000	0.000	0.000	0.000	0.000
Ti	0.035	0.073	0.091	0.020	0.021	0.181	0.024	0.092	0.064	0.093	0.060	0.050	0.067	0.080
Mg	1.426	1.369	1.406	1.429	1.661	1.673	1.587	1.653	1.739	1.695	1.705	1.702	1.608	2.099
Cr	0.004	0.005	0.006	0.003	0.002	0.000	0.000	0.002	0.004	0.003	0.003	0.000	0.006	0.002
Fe3	0.000	0.000	0.000	0.000	0.000	0.071	0.000	0.000	0.000	0.000	0.000	0.000	0.000	0.097
Fe2	0.927	0.955	0.965	1.012	0.905	0.970	0.924	0.947	0.854	0.952	0.944	0.887	0.902	0.690
Mn	0.002	0.005	0.000	0.012	0.012	0.012	0.007	0.009	0.008	0.010	0.009	0.007	0.013	0.009
Ca	0.167	0.132	0.176	0.042	0.073	0.197	0.063	0.161	0.132	0.129	0.120	0.120	0.142	0.214
Na	0.521	0.565	0.544	0.635	0.697	0.576	0.662	0.592	0.676	0.653	0.646	0.625	0.562	0.649
K	0.002	0.002	0.001	0.001	0.003	0.000	0.005	0.005	0.000	0.001	0.000	0.005	0.000	0.003
Mg#	0.61	0.59	0.59	0.59	0.65	0.62	0.63	0.64	0.67	0.64	0.64	0.66	0.64	0.73

(cont.)

Table 1. (continued)

Sample	SBJ														
	3B-1-2	3B-2-1	3B-2-2	3B-2-3	3B-3-1	3B-3-2	3B-4-1	3B-4-2	3B-4-3	3B-5	3B-6	3B-7	3B-10A	3B-14-1	3B-14-2
SiO_2	37.14	35.97	36.26	36.57	36.22	36.45	36.05	36.06	36.35	36.10	36.91	35.69	36.27	37.07	36.75
TiO_2	0.67	2.43	0.64	2.35	1.04	1.06	0.65	0.56	0.68	1.03	0.11	1.27	0.69	0.08	0.29
Al_2O_3	30.59	29.16	30.55	28.80	29.33	29.49	30.14	31.30	30.82	28.48	32.40	29.40	30.26	32.85	31.35
Cr_2O_3	0.07	0.00	0.08	0.05	0.01	0.00	0.01	0.05	0.03	0.15	0.01	0.00	0.00	0.00	0.02
FeO	5.21	7.83	5.50	7.71	5.60	5.89	5.89	6.02	5.85	5.51	5.81	5.89	5.71	5.88	5.13
MnO	0.05	0.08	0.06	0.08	0.06	0.07	0.07	0.07	0.06	0.05	0.05	0.06	0.03	0.04	0.09
MgO	9.25	7.62	9.19	7.73	9.95	9.65	9.17	8.37	8.48	9.91	7.91	9.38	9.12	7.52	9.06
CaO	1.62	1.03	1.61	1.21	2.79	2.96	1.91	0.95	1.30	2.91	0.65	2.34	1.72	0.52	0.91
Na_2O	1.85	2.21	1.92	2.14	1.35	1.39	1.69	2.28	2.08	1.35	2.42	1.56	1.94	2.12	2.16
K_2O	0.00	0.01	0.01	0.00	0.02	0.00	0.00	0.00	0.00	0.00	0.00	0.02	0.00	0.01	0.01
F	0.173	n.d	n.d	0.046	0.059	0.179	0.165	0.107	0.073	0.226	0.073	0.298	0.15	0.017	0.134
Cl	0.001	0.002	n.d	0.001	n.d	0.001	n.d	0.003	n.d	n.d	n.d	0.001	n.d.	n.d.	0.002
SiT	5.976	5.938	5.941	5.999	5.911	5.889	5.898	5.897	5.948	5.915	5.969	5.826	5.917	6.000	5.954
AlT	0.024	0.062	0.059	0.001	0.089	0.111	0.102	0.103	0.052	0.085	0.031	0.174	0.083	0.000	0.046
AlZ	5.778	5.614	5.841	5.568	5.554	5.505	5.712	5.930	5.894	5.417	6.000	5.482	5.738	6.000	5.943
AlY	0.000	0.000	0.000	0.000	0.000	0.000	0.000	0.000	0.000	0.000	0.147	0.000	0.000	0.273	0.000
SiY	0.000	0.000	0.000	0.000	0.000	0.000	0.000	0.000	0.000	0.000	0.000	0.000	0.000	0.006	0.000
Ti	0.081	0.302	0.078	0.290	0.128	0.129	0.080	0.069	0.084	0.127	0.014	0.155	0.085	0.010	0.036
Mg	2.218	1.874	2.244	1.890	2.420	2.322	2.237	2.041	2.069	2.420	1.906	2.282	2.218	1.814	2.189
Cr	0.009	0.000	0.010	0.006	0.002	0.000	0.002	0.006	0.004	0.019	0.001	0.000	0.000	0.000	0.003
Fe3	0.222	0.386	0.159	0.432	0.446	0.495	0.288	0.070	0.106	0.583	0.000	0.518	0.262	0.000	0.057
Fe2	0.479	0.695	0.594	0.626	0.318	0.300	0.518	0.753	0.695	0.172	0.785	0.287	0.517	0.797	0.638
Mn	0.006	0.012	0.008	0.011	0.008	0.010	0.009	0.009	0.008	0.007	0.006	0.008	0.005	0.005	0.012
Ca	0.278	0.182	0.282	0.212	0.488	0.512	0.335	0.166	0.228	0.511	0.112	0.410	0.300	0.090	0.157
Na	0.578	0.708	0.609	0.682	0.426	0.436	0.537	0.722	0.660	0.430	0.759	0.495	0.614	0.665	0.680
K	0.000	0.002	0.001	0.000	0.004	0.000	0.000	0.000	0.000	0.000	0.000	0.004	0.001	0.002	0.002
Mg#	0.76	0.63	0.75	0.64	0.76	0.74	0.74	0.71	0.72	0.76	0.71	0.74	0.74	0.69	0.76

(cont.)

Table 1. (continued)

Sample	SRJ													
	01-1	01-2	01-3a	01-3b	01-4	01-5	01-6	01-7	02-1	02-2	02-3	02-4	02-5	02-6
SiO_2	35.72	35.59	35.65	36.17	35.68	36.42	34.63	36.01	35.93	36.57	36.25	36.64	36.70	36.15
TiO_2	0.69	1.08	1.71	0.54	1.12	0.27	1.30	0.71	0.68	0.88	1.17	0.50	0.58	0.43
Al_2O_3	33.87	31.39	32.10	33.70	32.41	33.79	32.68	33.57	31.80	31.60	31.03	32.79	32.40	32.38
Cr_2O_3	n.d.	n.d.	n.d.	n.d.	n.d.	n.d.	n.d.	n.d.	n.d.	n.d.	n.d.	n.d.	n.d.	n.d.
FeO	9.40	7.74	8.57	8.47	8.19	8.66	8.99	8.42	6.54	6.69	6.50	6.52	5.84	5.00
MnO	0.06	0.12	0.04	0.06	0.10	0.10	0.09	0.09	0.06	0.04	0.05	0.06	0.02	0.03
MgO	4.99	6.63	5.80	5.40	6.40	5.41	5.33	5.74	7.68	8.24	8.66	7.57	8.33	8.40
CaO	0.75	1.11	1.24	0.55	1.08	0.51	0.78	0.67	0.79	0.80	1.46	0.53	0.83	0.81
Na_2O	1.82	1.89	1.66	1.95	2.01	1.88	1.74	1.86	2.42	2.41	2.08	2.40	2.35	2.38
K_2O	0.02	0.03	0.05	0.03	0.03	0.01	0.04	0.03	0.04	0.05	0.03	0.03	0.01	0.04
F	0.113	0.136	0.115	0.06	0.131	0.04	0.039	0.035	0.113	0.06	0.171	0.041	0.021	n.d.
Cl	n.d.	0.006	0.001	n.d.	n.d.	0.007	0.007	n.d.	n.d.	n.d.	0.002	0.006	0.001	0.001
SiT	5.796	5.865	5.817	5.876	5.798	5.908	5.757	5.848	5.868	5.901	5.836	5.906	5.909	5.899
AlT	0.204	0.135	0.183	0.124	0.202	0.092	0.243	0.152	0.132	0.099	0.164	0.094	0.091	0.101
AlZ	6.000	5.963	5.992	6.000	6.000	6.000	6.000	6.000	5.992	5.911	5.725	6.000	6.000	6.000
AlY	0.274	0.000	0.000	0.332	0.008	0.370	0.162	0.274	0.000	0.000	0.000	0.137	0.058	0.128
SiY	0.000	0.000	0.000	0.000	0.000	0.000	0.000	0.000	0.000	0.000	0.000	0.000	0.000	0.000
Ti	0.085	0.134	0.210	0.066	0.137	0.032	0.162	0.086	0.084	0.107	0.142	0.061	0.070	0.053
Mg	1.207	1.628	1.409	1.308	1.551	1.308	1.321	1.389	1.870	1.982	2.077	1.818	1.999	2.044
Cr	n.d.	n.d.	n.d.	n.d.	n.d.	n.d.	n.d.	n.d.	n.d.	n.d.	n.d.	n.d.	n.d.	n.d.
Fe3	0.000	0.037	0.008	0.000	0.000	0.000	0.000	0.000	0.008	0.089	0.275	0.000	0.000	0.000
Fe2	1.276	1.030	1.161	1.151	1.113	1.175	1.250	1.143	0.885	0.814	0.600	0.879	0.786	0.683
Mn	0.009	0.016	0.005	0.008	0.013	0.013	0.013	0.013	0.008	0.006	0.007	0.008	0.002	0.004
Ca	0.130	0.196	0.217	0.096	0.188	0.088	0.138	0.116	0.138	0.137	0.252	0.091	0.143	0.142
Na	0.571	0.603	0.525	0.615	0.632	0.592	0.560	0.585	0.767	0.755	0.649	0.749	0.733	0.752
K	0.003	0.007	0.010	0.005	0.007	0.001	0.008	0.007	0.009	0.009	0.006	0.006	0.002	0.008
Mg#	0.49	0.60	0.55	0.53	0.58	0.53	0.51	0.55	0.68	0.69	0.70	0.67	0.72	0.75

(cont.)

Table 1. (continued)

Sample	SRJ													
	04-1	04-2	04-3	04-4	04-5	04-6	05-1	05-2	05-3	05-4	08-1	08-2	08-3	08-4
SiO_2	36.07	35.53	35.17	35.90	35.49	35.68	36.59	35.76	35.62	35.80	36.44	35.98	36.27	36.45
TiO_2	0.78	0.77	1.03	0.63	0.28	1.02	0.14	0.87	0.83	0.48	0.70	0.25	0.59	0.14
Al_2O_3	35.10	35.20	34.16	34.46	34.79	33.61	34.27	33.84	33.78	34.72	32.35	33.54	32.92	33.10
Cr_2O_3	n.d.	n.d.	n.d.	n.d.	n.d.	n.d.	n.d.	n.d.	n.d.	n.d.	n.d.	n.d.	n.d.	n.d.
FeO	7.54	7.17	8.41	7.79	8.34	7.83	8.39	7.86	7.18	8.43	8.71	8.18	7.34	7.21
MnO	0.03	0.04	0.04	0.05	0.04	0.02	0.02	0.05	0.00	0.04	0.00	0.02	0.00	0.04
MgO	5.13	5.42	5.08	5.52	5.13	5.52	5.00	5.24	5.52	4.68	6.46	6.30	6.44	6.02
CaO	0.66	0.74	0.86	0.71	0.37	0.78	0.31	0.64	0.59	0.35	0.49	0.40	0.45	0.19
Na_2O	1.64	1.71	1.69	1.75	1.70	1.78	1.58	1.68	1.69	1.54	2.21	1.89	1.92	1.91
K_2O	0.02	0.02	0.01	0.04	0.03	0.02	0.00	0.03	0.02	0.04	0.03	0.04	0.03	0.02
F	0.075	0.113	0.055	0.077	0.039	0.093	0.019	0.018	0.036	n.d.	0.059	0.055	0.113	n.d.
Cl	n.d.	n.d.	0.009	0.001	n.d.	n.d.	0.001	0.001	n.d.	0.001	0.002	0.004	n.d.	n.d.
SiT	5.808	5.737	5.749	5.807	5.801	5.818	5.958	5.858	5.858	5.860	5.908	5.856	5.907	6.000
AlT	0.192	0.263	0.251	0.193	0.199	0.182	0.042	0.142	0.142	0.140	0.092	0.144	0.093	0.000
AlZ	6.000	6.000	6.000	6.000	6.000	6.000	6.000	6.000	6.000	6.000	6.000	6.000	6.000	6.000
AlY	0.473	0.438	0.332	0.379	0.507	0.278	0.537	0.395	0.408	0.560	0.092	0.290	0.228	0.428
SiY	0.000	0.000	0.000	0.000	0.000	0.000	0.000	0.000	0.000	0.000	0.000	0.000	0.000	0.003
Ti	0.095	0.093	0.126	0.077	0.034	0.124	0.017	0.107	0.103	0.059	0.085	0.031	0.072	0.017
Mg	1.231	1.305	1.237	1.332	1.251	1.341	1.214	1.279	1.354	1.142	1.560	1.527	1.563	1.478
Cr	n.d.	n.d.	n.d.	n.d.	n.d.	n.d.	n.d.	n.d.	n.d.	n.d.	n.d.	n.d.	n.d.	n.d.
Fe3	0.000	0.000	0.000	0.000	0.000	0.000	0.000	0.000	0.000	0.000	0.000	0.000	0.000	0.000
Fe2	1.015	0.968	1.150	1.054	1.140	1.068	1.142	1.077	0.988	1.154	1.181	1.114	1.000	0.993
Mn	0.004	0.006	0.005	0.007	0.005	0.003	0.003	0.007	0.000	0.005	0.000	0.003	0.000	0.005
Ca	0.113	0.127	0.151	0.123	0.064	0.137	0.055	0.112	0.103	0.061	0.085	0.070	0.079	0.034
Na	0.512	0.536	0.537	0.549	0.538	0.564	0.499	0.534	0.540	0.488	0.694	0.595	0.605	0.611
K	0.005	0.003	0.003	0.009	0.006	0.003	0.000	0.007	0.005	0.009	0.006	0.008	0.007	0.005
Mg#	0.55	0.57	0.52	0.56	0.52	0.56	0.52	0.54	0.58	0.50	0.57	0.58	0.61	0.60

tourmaline, richer in MgO and Na_2O and poorer in Al_2O_3 and FeO, may reflect the compositional variation of the rock from which it is crystallizing from (e.g., amphibolitic intercalations in schist);

2. tourmaline from SJB-3A, with average Mg# = 0.64, intermediate Al_2O_3 and FeO contents to SRJ and SJB-3B tourmaline compositions, and slightly lower CaO and higher Na_2O contents relative to SRJ tourmalines;

3. tourmaline from SJB-3B, with Mg# > 0.7, the lowest Al_2O_3 and FeO contents, low Na_2O contents and high CaO and F contents.

REE and trace elements by ICP-MS

The ICP-MS analyses of REE and trace elements for the SRJ, SJB-3A and SJB-3B tourmaline separates are presented in Table 2. For comparison, C1 chondrite-normalized REE (REE_{CN}) patterns yielded by these tourmalines are represented in Figure 5 together with the results obtained by Pereira (2001) for three samples (whole rock) from the São José do Barreiro Granite.

The total REE contents vary widely from 3.51 ppm (SJB-3A, taking into account that HREE contents are below the ICP-MS detection limits) to 305 ppm (SJB-3B).

The SRJ tourmalines (total REE contents from 8 to 58 ppm) define two distinct REE_{CN} patterns: *pattern 1*, characterized by positive Eu anomalies and REE enrichment up to 10 times the chondrite values [$(La/Yb)_{CN}$ = 2.7 - 4.1], and *pattern 2*, characterized by no evident Eu anomaly and HREE enrichment from 10 to 80 times the chondrite values [$(La/Yb)_{CN}$ = 0.2 - 0.3]. Sample SRJ-02 tourmaline, although showing differences in major element composition in relation to the other SRJ tourmalines, yields a very similar REE_{CN} pattern to *pattern 1* and $(La/Yb)_{CN}$ = 4.3. The REE_{CN} pattern for SRJ-04 is also characterized by a positive Eu anomaly, but is *ca*. three times more enriched in REE than those that define *pattern 1* and $(La/Yb)_{CN}$ = 1.3.

Bau (1991), analyzing REE mobility during fluid-rock interaction related to hydrothermal alteration and metamorphism, takes into account temperature, pH, f_{O2} and (primary and secondary) mineral/liquid partition coefficients to explain the resulting REE patterns for the altered rock and the fluid. For europium in particular, temperature and pH can influence the Eu^{3+}/Eu^{2+} redox potential. Thus, provided the temperature is high enough, Eu can occur in the divalent oxidation state, even in mildly reducing environments. The change of valence state is accompanied by an increase in ionic radius (HREE Lu^{3+} = 0.861 Å < Eu^{3+} = 0.947 Å < LREE La^{3+} = 1.032 Å < Eu^{2+} = 1.17 Å) and an Eu anomaly will result in the REE pattern, because Eu will behave differently (as a LFSE) from the other REE (HFSE) in that geochemical system. In fluid-rock interactions, the REE pattern of the fluid phase may be governed by: 1) the REE pattern of the rock the fluid is in contact with (e.g., breakdown of primary and/or precipitation of secondary minerals, causing changes in the mineral/fluid REE partition coefficients); 2) sorption (stronger sorption on mineral or particle surfaces lowers

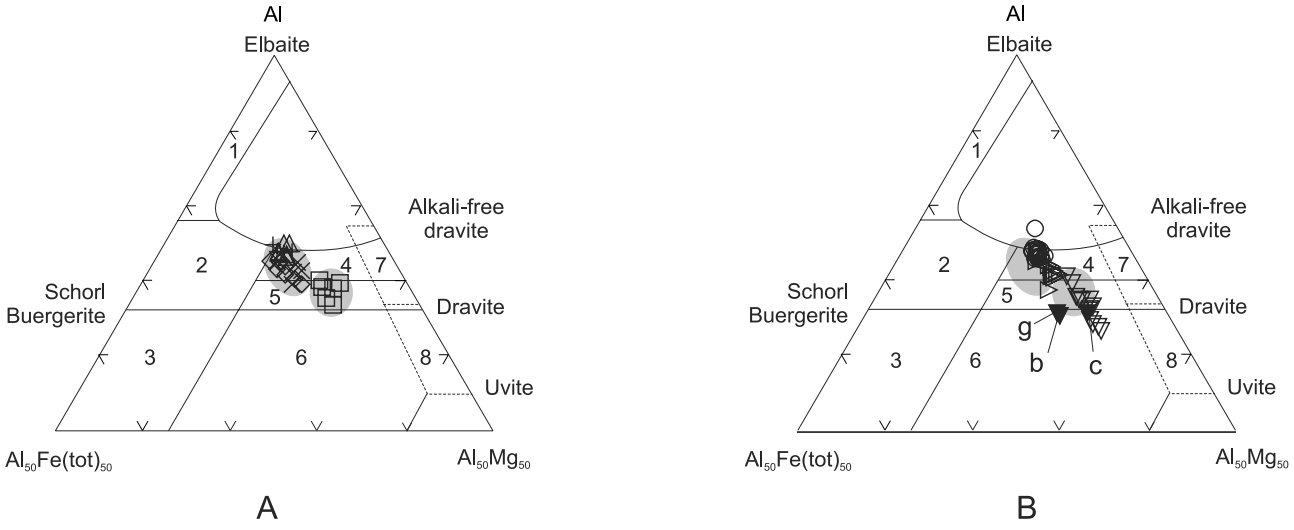

Figure 3. Henry and Guidotti (1985) Fe-Al-Mg diagram (atomic proportions). Numbered fields: **1.** Li-rich granitoid pegmatites and aplites; **2.** Li-poor granitoids and their associated pegmatites and aplites; **3.** Fe^{3+}-rich quartz-tourmaline rocks (hydrothermally altered granites); **4.** metapelites and metapsammites coexisting with an Al-saturating phase; **5.** metapelites and metapsammites not coexisting with an Al-saturating phase; **6.** Fe^{3+}-rich quartz-tourmaline rocks, calc-silicate rocks, and metapelites; **7.** low-Ca metautramafics and Cr, V-rich metasediments; **8.** metacarbonates and metapyroxenites. Symbols as in Figure 4.

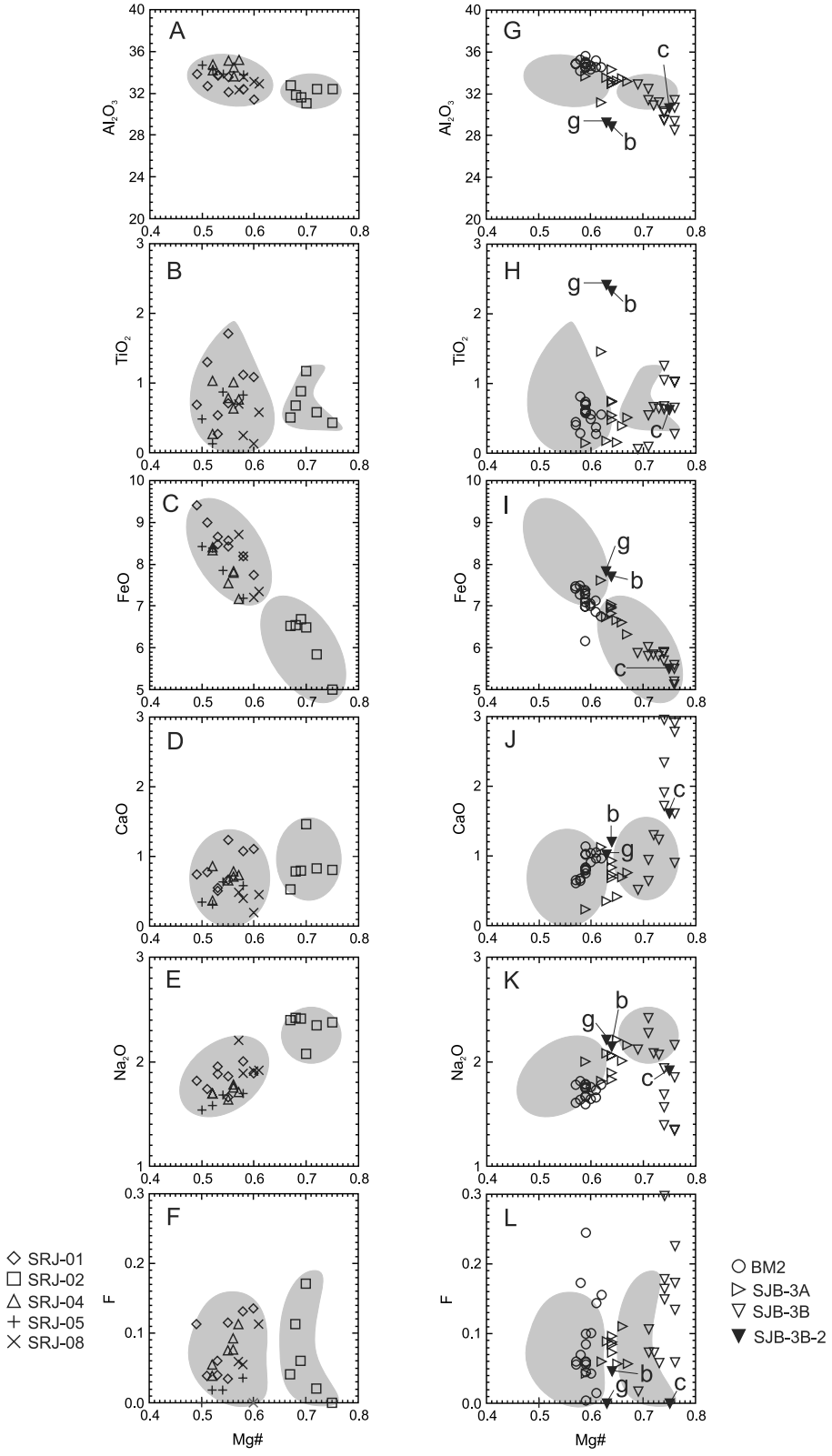

Figure 4. Compositional variations in SRJ (left) and BM2, SJB-3A and SJB-3B (right). Fields in gray represent SRJ analyses.

Table 2. ICP-MS data for samples SRJ, SJB-3A and SJB-3B (ppm).

	SRJ-01	SRJ-02	SRJ-03	SRJ-04	SRJ-05	SRJ-08	SJB-3A	SJB-3B
La	2.12	2.22	1.75	8.12	4.01	1.64	0.78	45.8
Ce	3.51	3.40	2.97	16.6	6.90	3.35	1.57	117
Pr	0.41	0.35	0.30	1.85	0.87	0.43	0.13	15.6
Nd	1.40	1.17	0.98	6.70	3.17	1.65	0.5	67.8
Sm	0.26	0.25	0.18	1.29	1.34	0.48	0.09	15.3
Eu	0.62	0.32	0.56	1.40	1.05	0.44	0.17	3.22
Gd	0.31	0.30	0.20	1.49	3.77	1.35	0.07	12.9
Tb	0.06	0.06	0.05	0.35	1.10	0.40	0.01	1.9
Dy	0.46	0.43	0.31	3.05	9.41	3.64	0.06	10.4
Ho	0.12	0.10	0.07	0.96	2.57	1.03	0.01	2
Er	0.41	0.31	0.23	3.62	8.75	3.31	0.04	5.51
Tm	0.07	0.05	0.04	0.66	1.61	0.54	0.01	0.82
Yb	0.56	0.37	0.31	4.64	11.8	3.64	0.06	5.65
Lu	0.10	0.06	0.06	0.77	1.86	0.56	0.01	0.85
Rb	0.38	0.21	0.11	0.10	0.34	0.10	0.32	0.26
Sr	201	242	193	114	118	250	203	258
Y	3.51	2.37	1.79	23.9	83.3	23.9	0.44	50.5
Zr	130	35.1	52.7	185	55.2	211	16.9	778
Nb	1.32	1.39	0.89	2.16	0.97	14.4	0.23	1.81
Cs	0.04	0.02	0.01	0.01	0.02	0.01	0.03	0.03
Ba	5.16	5.80	2.37	2.35	4.81	1.65	2.69	2.75
Hf	3.93	1.34	2.15	7.05	2.74	7.93	0.53	20
Ta	0.21	0.20	0.15	0.42	0.27	1.92	0.06	0.2
Pb	15.8	6.89	12.1	12.5	14.2	14.4	7.07	4.68
Th	0.49	0.88	0.29	1.49	1.93	1.11	0.1	6.36
U	0.37	0.24	0.26	0.46	2.55	0.61	0.07	1.76

the amount of a REE in the fluid), and 3) chemical complexation reactions (stronger complexation increases the amount of a REE in the fluid because of the higher solubility of REE complexes compared to uncomplexed REE species).

An example of sorption processes affecting the REE pattern of the fluid phase given by Bau (1991) is the high-temperature (≈350 °C) MORB alteration at pH ≈3.8 (mildly acidic condition). Because f_{O2} is below the related SO_4^{2-}/H_2S equilibrium, europium occurs as Eu^{2+} and the fluid REE_{CN} pattern is characterized by a positive Eu anomaly and $(La/Lu)_{CN} > 1$. Because Fe and Al in such seafloor environment will compete for F^- or Cl^-, REE complexation is not favored and still uncomplexed REE species will be present in the fluid.

On the other hand, lower temperatures (≈130 °C), pH between 6.7 and 7.3, and complexation by mono- and bicarbonates (example also in Bau, 1991), can prevent Eu^{3+} from being reduced to Eu^{2+} (as the stability of Eu^{3+} is extended towards lower f_{O2}), resulting in no Eu anomaly and La/Lu ratio < 1.

Tourmaline is only stable in strong-to-weakly acid solutions (Henry and Dutrow, 1996; Palmer and Swihart, 1996). The rock must have the appropriate bulk composition to form tourmaline by metamorphism so that any boron intrinsic to the rock or introduced into the rock can react with the requisite chemical constituents to develop tourmaline. Temperature, pressure and fluid composition should be appropriate to stabilize tourmaline (Henry and Dutrow, 1996). According to Bau (1991), the REE content in metamorphic fluids can increase with increasing temperatures because of a greater availability of complexing agents like F^-, CO_3^{2-}, or OH^-. If the fluid/rock ratio is high enough, fluid-rock interaction will lead to the preferential removal of HREE from the rock, due to the predominance of F^-, CO_3^{2-}, or OH^- complexes in the metamorphic fluid. Because selective enrichment or removal of Eu is unlikely under these geochemical

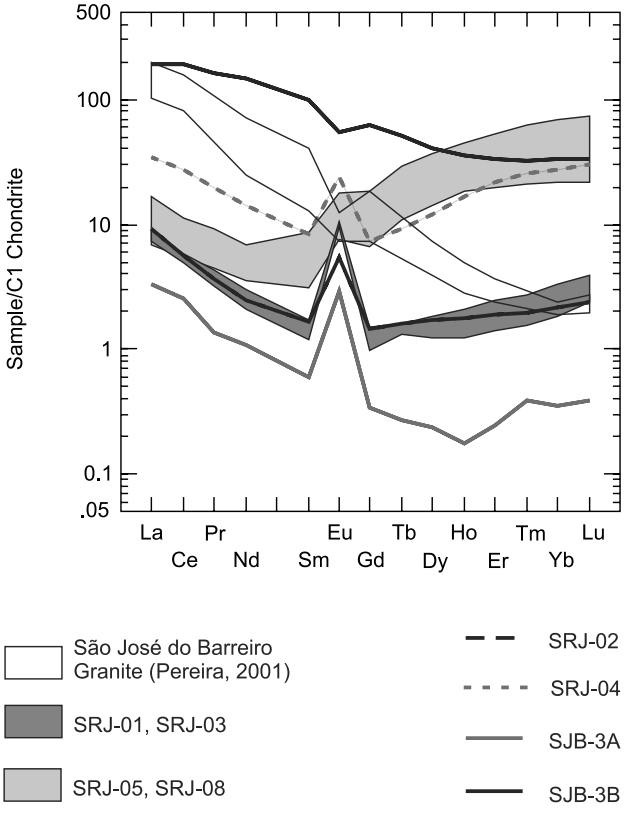

Figure 5. REE concentrations normalized to Chondrite C1 (Sun and McDonough, 1989).

conditions, the tourmaline that precipitates from this fluid will yield a REE_{CN} pattern characterized by $(La/Lu)_{CN} < 1$ and no Eu anomaly (our *pattern 2*).

Therefore, our *pattern 1* and *pattern 2* can be explained by the evolution of the metamorphic fluid from lower to higher temperatures, with increasing HREE content due to complexation by F^-, CO_3^{2-}, or OH^-, and the change of signature, from a positive to practically no Eu anomaly. Whereas the major element composition of the SRJ tourmalines reflects the composition of the rocks from which the tourmalines are forming (Una Unit schists), the REE patterns for these tourmalines illustrate how the metamorphic fluid evolved with changing metamorphic conditions.

The tourmaline of the thin SJB-3A tourmalinite intercalated in the *saibreira* is the least REE-enriched, showing a positive Eu anomaly and HREE concentrations below the ICP-MS detection limits, which can be explained by high fluid/rock ratios and reducing conditions discussed above, or, better yet, considering a possible interference of magmatic-hydrothermal fluids from the São José do Barreiro Granite, such a $(REE)_{CN}$ pattern may indicate that tourmaline derived from exsolved fluids from the magma rather than directly crystallizing from the silicate melt, once such fluids are poorer in REE relative to corresponding melt-derived tourmaline (Jolliff, Papike, Laul, 1987; Pesquera et al., 2005). On the other extreme and differing from all the other patterns, sample SJB-3B yields a slightly negative Eu anomaly and $(La/Yb)_{CN} = 5.8$.

Pesquera et al. (2005) obtained very similar REE patterns to SJB-3A and SJB-3B for tourmalines from tourmalinites of the Martinamor Anticline (Salamanca, Spain). Relative to the whole rock, tourmalines from tourmalinites (which also contain quartz, plagioclase, muscovite, biotite, apatite, rutile, and zircon) exhibit: a) depletion of LFSE such as Rb, Cs and Ba that are preferentially partitioned into micas and feldspar; b) higher Li, Sc, V, Zn and Ga, but lower Cr, Ni, Co, Sn, W, Y, and HFSE, including Zr, Hf, Nb and Ta, the latter probably controlled by the distribution of zircon (Zr and Hf), rutile (Nb and Ta) and monazite (REE); and c) lower HREE-contents. The differences in REE patterns are explained by differential fluid/rock ratios during metasomatic processes: tourmalines with low REE abundances and positive Eu anomalies are considered to reflect deposition under relatively high fluid/rock ratios in comparison with those that have high REE abundances.

Similar to the Martinamor Anticline tourmalinites, the SJB-3B tourmaline also stands out for comparatively high HFSE concentrations, such as Th (6.36 ppm), U (1.76 ppm), Hf (20 ppm), Zr (778 ppm), and total REE contents (304.8 ppm). It also contains comparatively high Sr (258 ppm) concentrations.

The $(REE)_{CN}$ pattern for SJB-3B resembles that of the strongly REE-fractionated São José do Barreiro Granite (Pereira, Moura, Bustamante-Junho, 2002), which may indicate contribution from magmatic-hydrothermal fluids.

It is worth mentioning that depletion of Rb, Cs and Ba is observed in all samples (respectively 0.10 - 0.38 ppm, 0.01 - 0.04 ppm, and 1.65 - 5.80 ppm).

Boron isotopes by SIMS

Unfortunately the SRJ tourmalines mounted in epoxy resin could not be further analyzed for boron isotopes by SIMS, because of the interference of the resin volatilization in the analyses. Thus, only tourmalines in polished thin sections were analyzed and, as seen in Table 3, all of the 12 boron isotope analyses yielded negative $\delta^{11}B$ values with a total range from -12.3‰ to -13.9‰ (average of -13.1‰) for SJB-3A and -13.9‰ to -15.8‰ for SJB-3B (average of -14.7‰).

The $\delta^{11}B$ values obtained in this study fall in the -15 to -5‰ interval compiled by Marschall and Ludwig (2006) for tourmaline related to S-type granite magmatism,

which is in accordance with our REE results, indicating relationship between the REE-rich fluids that originated the SBJ-3B tourmalines with the evolution of S-type São José do Barreiro Granite.

Boron has no natural redox chemistry, so fractionation between the two isotopes ^{10}B and ^{11}B is almost entirely controlled by their relative partitioning between trigonal, such as $B(OH)_3$, and tetragonal species, such as $B(OH)_4^-$ (Palmer and Swihart, 1996). Boron is very mobile during fluid-rock interactions and is significantly partitioned into vapor during phase separation. For example, Cl-rich geothermal fluids are depleted in ^{11}B due to partitioning of ^{11}B-enriched, trigonally-coordinated boron into the vapor phase (Slack, 1996).

According to Jiang et al. (2008), tourmaline can, in magmatic systems, crystallize directly from the melt or from exsolved hydrothermal fluids, and can span a large range in $\delta^{11}B$ values, from -30 to +9‰. Boron isotope data can indicate whether the tourmaline crystallized directly from a melt or during late magmatic-hydrothermal activity once: a) minimal boron isotope fractionation occurs between melt and tourmaline at magmatic temperatures, so that the $\delta^{11}B$ of magmatic tourmaline should approximate that of the parental granitic magma; b) during magmatic evolution and degassing and because $B(OH)_3$ is volatile, the exsolved fluids become enriched in ^{11}B, leading to an increase in the $\delta^{11}B$ of the tourmaline that precipitate from them, or a $\delta^{11}B$ decrease from core to rim of tourmaline crystallizing from the magma, as it undergoes depletion in ^{11}B during tourmaline growth; c) tourmalines forming during a single magmatic-hydrothermal stage, with boron-rich fluids being exsolved from the granitic melt, may show clear compositional differences between the cores and rims but their boron isotopic compositions remain the same (had tourmaline formed during the magmatic stage, boron isotope fractionation between the early- and later-stage tourmaline would be expected); d) involvement of a local metamorphic fluid that mixes with magmatic-hydrothermal fluids is suggested by slightly lower $\delta^{11}B$ values (together with increase in Mg contents) at rims in comparison with the cores of tourmalines; e) during both prograde and retrograde metamorphism, changes in the temperature and chemistry of circulating fluids may affect the geochemical and $\delta^{11}B$ values of the tourmaline.

The involvement of metamorphic fluids with magmatic-hydrothermal fluids is indicated by the slightly more negative $\delta^{11}B$ obtained for SJB-3B, which is also more Mg-enriched, than SJB-3A (alternative (d) of Jiang et al., 2008).

Table 3. Boron isotope analyses by SIMS of tourmalines from São José do Barreiro.

Sample	Grain	$^{11}B/^{10}B$	$\delta^{11}B$‰
SJB-3A	t1	3.994	-12.31
SJB-3A	t2	3.991	-13.01
SJB-3A	t3	3.988	-13.72
SJB-3A	t4	3.987	-13.90
SJB-3A	t5	3.992	-12.79
SJB-3B	t1	3.980	-15.76
SJB-3B	t2	3.988	-13.88
SJB-3B	t3	3.982	-15.36
SJB-3B	t4	3.985	-14.51
SJB-3B	t5	3.985	-14.43
SJB-3B	t6	3.987	-14.10

RUTILES

Materials and methods

During the separation of tourmaline from sample SJB-3B, rutile was identified in the 100 - 150 mesh fraction. Rutile prisms are either dark red or green or of both colors and they concentrate in the magnetic fraction of the Frantz separator together with tourmaline. The separates were cleaned from sulfides by chemical attack with HNO_3 (50%) for 72 hours and quartz was removed using dense liquids.

The rutile separates were mounted in epoxy resin, polished and coated with carbon. Back-scattered electron (BSE) images and semi-quantitative (EDS) analyses were obtained at the *Laboratório de Caracterização Tecnológica* (São Paulo University), equipped with a LEO 440 scanning electron microscope coupled with an OXFORD Isis 300 EDS System. Quantitative (WDS) analyses were performed at the *Instituto de Geociências* with the JEOL JXA-8600 microprobe operating under the following conditions: beam diameter 5 μm, beam current 120 nA and acceleration voltage 20 kV.

Chemical composition of retiles

BSE images and EDS and WDS analyses

Back-scattered electron (BSE) images of rutile crystals and semi-quantitative EDS analyses obtained with the scanning electron microscope helped associate different shades of gray in the BSE images with variations in composition within single crystals. Lighter shades in the BSE images correspond to increase in Fe, Sn, W and Nb contents, as indicated in Figure 6 by arrows.

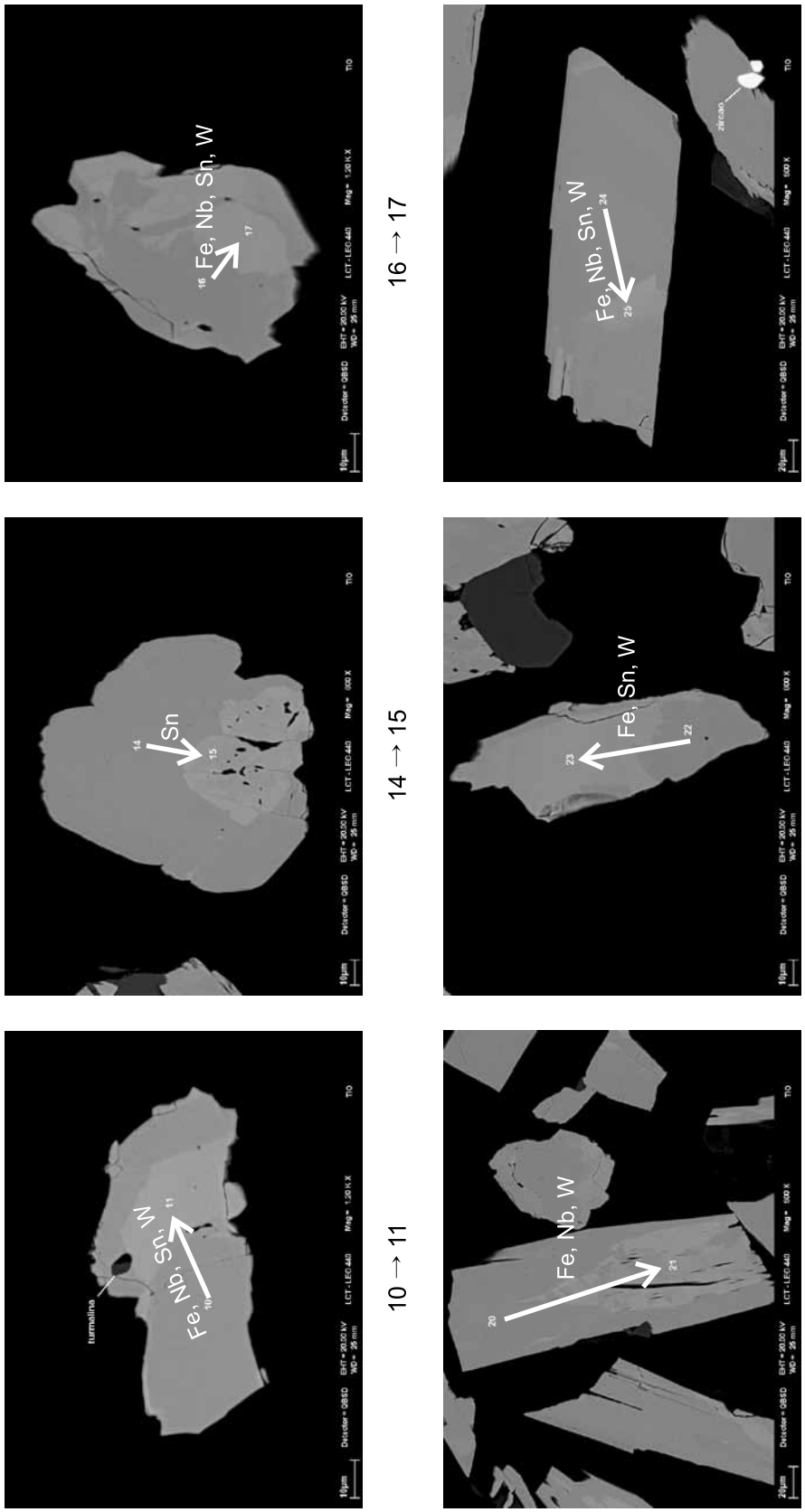

Figure 6. BSE images of SJB-3B rutile crystals. Arrows indicate composition variations from "darker" (even numbers) to "lighter" (odd numbers) zones of a single crystal.

Quantitative WDS analyses were carried out in red and green parts of rutile crystals mounted in epoxi resin and the results are presented in Table 4.

Average TiO_2 content in red rutiles is 96 wt.% (±1 wt.%), whereas in green rutiles it is slightly lower, 95 wt.% (±2 wt.%). Cr contents in green rutiles are restricted to the 443 - 1007 ppm interval, whereas in red rutiles they vary between 2392 and 6497 ppm. On the other hand, Nb contents in red rutiles fall in the 3910 - 5203 ppm interval, whereas they vary from 2000 to 7500 ppm in green rutiles (Figure 7A). The contents of Si (Figure 7C); Al (Figure 7D); Fe (Figure 7E), and Sn (Figure 7G) are higher in green than in red rutiles.

As mentioned before, rutile chemistry and thermometry has been used as a guide to provenance for a variety of geological settings. For example, Zack, Moraes and Kronz (2004b) observed an important correlation between Zr content in rutile and metamorphic peak and devised a

Table 4. Microprobe (WDS) analyses of SJB-3B rutile separates. Labels SJB-3B-V and SJB-3B-P indicate green and red rutile respectively. Ti contents in wt.% and trace elements contents in ppm.

Sample	Ti wt.%	Si	Cr	Al	Nb	Fe	V	Zr	Sn
SJB-3B-V02	58.44	174	968	368	2192	1941	1391	113	11201
SJB-3B-V03	57.29	0	769	765	6758	7023	1821	112	15368
SJB-3B-V04	58.34	418	774	435	2537	1871	1328	226	11933
SJB-3B-V05a	57.55	0	449	733	5505	6549	1446	113	14654
SJB-3B-V05b	58.43	35	1228	268	6238	3958	1710	454	3985
SJB-3B-V06	58.14	70	902	468	3455	2492	1642	113	12801
SJB-3B-V07	58.03	383	1225	769	2995	2215	1895	113	13392
SJB-3B-V08	57.68	69	449	366	4128	3791	1320	225	17876
SJB-3B-V09	56.75	69	446	496	4897	4724	1436	112	28086
SJB-3B-V10	58.24	174	322	469	2996	2840	1706	113	12074
SJB-3B-V12-1	56.95	0	640	1062	6629	9480	1943	224	16940
SJB-3B-V12-2	56.93	0	576	896	6513	10165	1942	224	16790
SJB-3B-V13	56.54	69	956	694	5692	6295	1810	112	26909
SJB-3B-V14	58.48	35	970	403	4158	3194	1900	227	6493
SJB-3B-V15	58.08	174	838	368	4720	2976	1389	339	11915
SJB-3B-V16	57.38	35	320	599	5152	5988	1507	112	18141
SJB-3B-V21	56.93	35	767	962	6740	9889	1629	112	17079
SJB-3B-V22	58.1	70	644	502	4030	3183	1704	113	12210
SJB-3B-V23-1	58.42	139	1162	435	2538	1941	1328	227	10759
SJB-3B-V25	57.09	0	1089	897	7208	7359	1819	112	16520
SJB-3B-P01	58.36	35	2908	302	4156	2637	1773	453	6491
SJB-3B-P02	58.56	0	2135	302	4046	2779	1775	341	4874
SJB-3B-P03	58.38	35	4591	201	4274	1597	1710	340	5609
SJB-3B-P04	58.27	70	1614	335	5306	2982	1771	n.d.	7959
SJB-3B-P05	58.31	0	3813	402	4619	3609	1836	227	4722
SJB-3B-P06a	58.11	35	4840	268	4497	3119	1770	113	7072
SJB-3B-P06b	58.43	105	2458	268	4853	2987	1837	454	4725
SJB-3B-P07	58.1	0	7300	302	5541	1457	1646	453	4720
SJB-3B-P08	58.45	35	1292	369	3117	3539	1772	113	7670
SJB-3B-P11	58.27	0	4588	201	5772	2221	1456	453	5015
SJB-3B-P12	58.37	0	5562	201	4160	1459	1711	454	4725
SJB-3B-P13	58.41	0	5886	168	4392	1181	1457	227	4578
SJB-3B-P14	58.18	0	8660	134	4041	763	1583	227	5164
SJB-3B-P15	58.26	0	3422	268	3577	3121	1835	113	7666

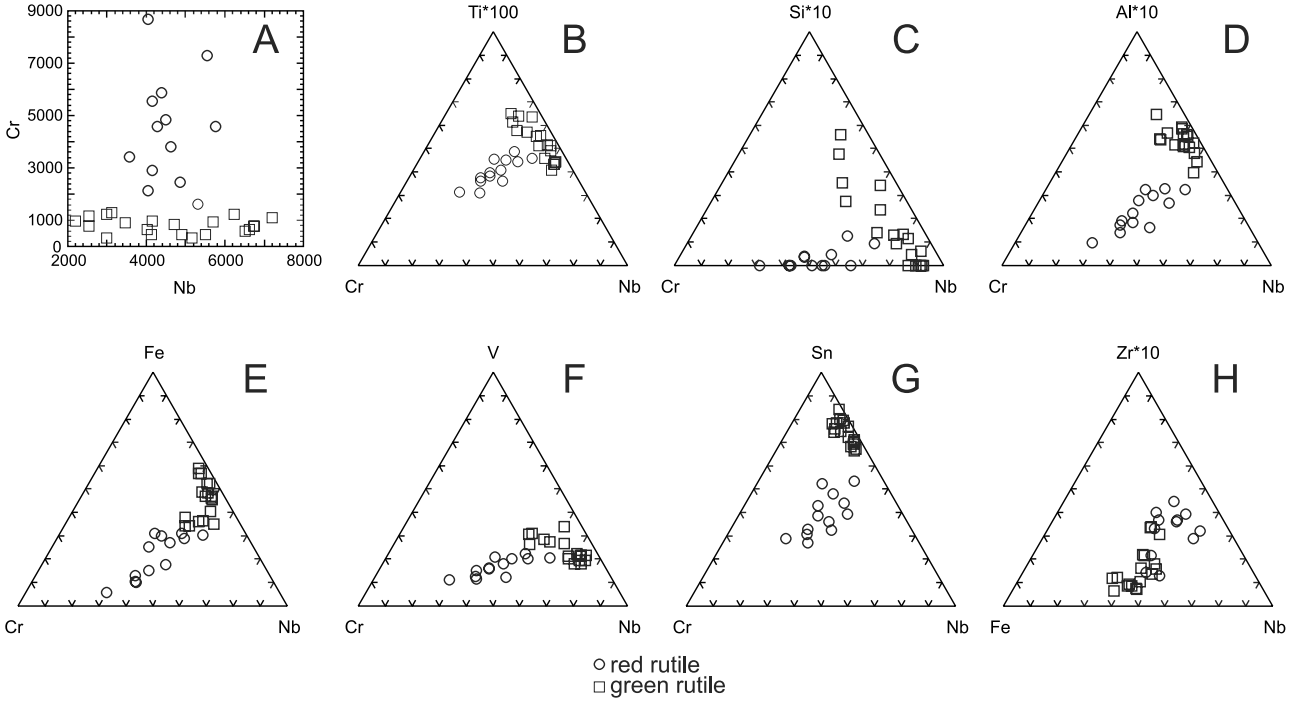

Figure 7. Chemical variation diagrams for red and green rutiles from sample SJB-3B.

geothermometer with possible applications covering the fields of ultrahigh temperature granulites, sedimentary provenance studies and metamorphic field gradients. Watson, Wark and Thomas (2006) presented a revised Zr-in-rutile thermometer based on experimental data and natural rutiles from metamorphic rocks.

Fernández, Schalamuk and Omenetto (2005), based on Fe, Sn, Nb, Ta and W contents in rutile from greisenized host rock and vein-related greisen of the Sn-W Mazan District (Argentina), distinguish two different greisen-forming conditions. The authors propose that the rutile present in the vein-related greisen fundamentally formed from Ti-bearing hydrothermal solutions (at high fluid/rock ratios), whereas the rutile of the greisenized host rock formed at the expense of Ti liberated during the destruction of rock minerals (at low fluid/rock ratios). At high fluid/rock ratios, cassiterite and wolframite deposited together with rutile.

According to Force (1980), hydrothermally or metasomatically altered rocks commonly contain rutile (porphyry copper deposits, wallrocks of metamorphosed massive sulfide deposits, metamorphosed ultramafic rocks), and, although rare in granitic pegmatites because of the low TiO_2 contents of residual melts, it is a common phase in the country rocks. Therefore, both medium- to high-grade metamorphism and hydrothermal activity can mobilize Ti from country rocks to produce rutile. It is possible that the red rutile at predominant high rock/fluid ratios, whereas green rutile formed at low rock/fluid ratios, a possible source of magmatic-hydrothermal fluids being the São José do Barreiro Granite. The Ti-rich zones in coarse-grained tourmaline (Figure 2C and Figure 7H) may correspond to changes in fluid composition. Other minerals, such as zircon, monazite and scheelite (identified in BSE images of rutile separates), may have precipitated under these conditions.

As further mechanism of Sn and W incorporation by rutile, Müller and Halls (2005) suggested the contribution from relatively oxidizing formation waters reacting with the magmatic residue, based on the high Fe (Sn, W) in the final outer growth zones of rutile and tourmaline of the tourmaline breccia at Wheal Remfry (SW England). Considering the geologic setting of the study area, it is possible that meteoric waters also played a role in rutile and tourmaline formation, but the data obtained is not enough to attest the involvement of fluids other than metamorphic and (post-) magmatic.

CONCLUSIONS

Tourmaline and rutile geochemistry helped distinguish two main phases of tourmaline formation in tourmaline-rich layers intercalated with the Embu Complex aluminous

schists and with quartzite (*saibreiras*) of the São José do Barreiro-Formoso region.

The tourmalines of the schist-hosted tourmaline layers are characterized by relatively low MgO, Na_2O and CaO contents and high Al_2O_3 and FeO contents. Two $(REE)_{CN}$ patterns were defined for these tourmalines, one represented by $(La/Yb)_{CN}$ from 2.7 to 4.3 and positive Eu anomalies, and the other by $(La/Yb)_{CN}$ from 0.2 to 0.3 and practically no Eu anomalies. The variations in major-element contents reflect the composition of the metamorphic rock in which the tourmaline is crystallizing, whereas the $(REE)_{CN}$ patterns indicate the evolution of the metamorphic fluids with increasing temperatures.

The tourmaline of the tourmalinite layer intercalated in quartzite is characterized by relatively high Al_2O_3, FeO and Na_2O contents and very low total REE contents. Its $(REE)_{CN}$ pattern is characterized by a positive Eu anomaly. $\delta^{11}B$ values for this tourmaline fall in the -12.3 and -13.9‰ interval. On the other hand, the tourmaline of a massive tourmalinite has the highest MgO, CaO, F, Th, U, Hf, Zr, Y, Sr and total REE contents and the lowest Al_2O_3 and FeO contents. Differing from all other $(REE)_{CN}$ patterns, the one that characterizes this tourmaline is LREE-enriched [$(La/Yb)_{CN}$ = 5.8] and shows a slightly negative Eu anomaly. $\delta^{11}B$ values in the -13.9 and -15.8‰ interval indicate an S-type granite filiation.

The green rutile of the massive tourmalinite is enriched in Nb, Al, Fe and Sn when compared to the Cr-rich red rutile. The differences in composition observed in the tourmaline and rutile of the massive tourmalinite indicate the involvement of magmatic-hydrothermal fluids from the S-type São José do Barreiro Granite with metamorphic fluids from which tourmaline crystallized.

The formation of zircon, scheelite, and monazite in the massive tourmalinite must be related to this second phase of tourmaline crystallization. Fluid inclusion studies may attest for both change in fluid composition and metal (Sn, W, and Nb) deposition.

ACKNOWLEDGMENTS

The authors wish to thank FAPESP (Processes 2005/56651-3 and 2007/53895-4) for financial support for this project. G. M. Garda and P. Beljavskis are greatly indebted to Ronaldo M. Pereira for the SRJ tourmaline separates, to Marcos S. Mansueto for his assistance during microprobe analyses, to Margaret S. Navarro for trace element analyses by ICP-MS, and to Dr. Robert B. Trumbull from GFZ Potsdam, for monitoring sample preparation and SIMS analyses and for the extremely critical review of the first drafts of this manuscript. G. M. Garda also wishes to thank FAPESP (Process 2010/50768-4) for the opportunity to present a poster on this paper in the IMA2010 Meeting (Bonds and Bridges: Mineral Sciences and Their Applications) in Budapest (Hungary).

REFERENCES

BAU, M. Rare-earth element mobility during hydrothermal and metamorphic fluid-rock interaction and the significance of the oxidation state of europium. *Chemical Geology*, v. 93, p. 219-230, 1991.

BORTNIKOV, N. S.; GORELIKOVA, N. V.; KOROSTELEV, P. G.; GONEVCHUK, V. G. Rare earth elements in tourmaline and chlorite from tin-bearing assemblages: Factors controlling fractionation of REE in hydrothermal systems. *Geology of ore deposits*, v. 50, n. 6, p. 445-461, 2008.

CATANZARO, E. J.; CHAMPION, C. E.; GARNER, E. L.; MALINENKO, G.; SAPPENFIELD, K. M.; SHIELDS, W. R. *Boric acid: isotopic and assay standard reference materials*. Washington, D. C.: US National Bureau Standards, Special Publication 260-17, 70 p. 1970.

DYAR, M. D.; WIEDENBECK, M.; ROBERTSON, D.; CROSS, L. R.; DELANEY, J. S.; FERGUSON, K.; FRANCIS, C. A.; GREW, E. S.; GUIDOTTI, C. V.; HERVIG, R. L.; HUGHES, J. M.; HUSLER, J.; LEEMAN, W.; McGUIRE, A. V.; RHEDE, D.; ROTHE, H.; PAUL, R. L.; RICHARDS, I.; YATES, M. Reference minerals for microanalysis of light elements. *Geostandard Newsletter*, v. 25, p. 441-463, 2001.

FERNÁNDEZ, R. R.; SCHALAMUK, I. B. A.; OMENETTO, P. Composición del rutilo como indicador de las condiciones de formación del *greisen* del distrito Mazán (Sn-W), provincia de La Rioja. *Revista de la Asociación Geológica Argentina*, v. 60, p. 259-267, 2005.

FORCE, E. R. The provenance of rutile. *Journal of Sedimentary Petrology*, v. 50, p. 485-488. 1980.

GARDA, G. M.; TRUMBULL, R. B.; BELJAVSKIS, P.; WIEDENBECK, M. Boron isotope composition of tourmalinite and vein tourmalines associated with gold mineralization, Serra do Itaberaba Group, central Ribeira Belt, SE Brazil. *Chemical Geology*, v. 264, p. 207-220. 2009.

HASUI, Y.; OLIVEIRA, M. A. F. Província Mantiqueira - setor central. In: ALMEIDA, F. F. M.; HASUI, Y.

(Coord.). *O Pré-Cambriano do Brasil.* São Paulo: Edgar Blucher, 1984. p. 308-344.

HENRY, D. J.; DUTROW, B. L. Metamorphic tourmaline and its petrogenetic applications. In: GREW, E. S.; ANOVITZ, L. M. (Ed.). *Boron*: mineralogy, petrology and geochemistry. Chantilly, Va.: Mineralogical Society of America, 1996. p. 503-557. (Reviews in Mineralogy, v. 33).

HENRY, D. J.; GUIDOTTI, C. V. Tourmaline as a petrogenetic indicator mineral: an example from the staurolite-grade metapelites of NW Maine. *American Mineralogist*, v. 70, p. 1-15, 1985.

JIANG, S. Y.; RADVANEC, M.; NAKAMURA, E.; PALMER, M.; KOBAYASHI, K.; ZHAO, H. X.; ZHAO, K. D. Chemical and boron isotopic variations of tourmaline in the Hnilec granite-related hydrothermal system, Slovakia: constraints on magmatic and metamorphic fluid evolution. *Lithos*, v. 106, p. 1-11, 2008.

JOLLIFF, B. L.; PAPIKE, J. J.; LAUL, J. C. Mineral recorders of pegmatite internal evolution: REE contents of tourmaline from the Bob Ingersoll pegmatite, South Dakota. *Geochimica et Cosmochimica Acta*, v. 51, p. 2225-2232, 1987.

MARSCHALL, H. R.; LUDWIG, T. Re-examination of the boron isotopic composition of tourmaline from the Lavicky granite, Czech Republic, by secondary ion mass spectrometry: back to normal. *Geochemical Journal*, v. 40, p. 631-638, 2006.

MEINHOLD, G.; ANDERS, B.; KOSTOPOULOS, D.; REISCHMANN, T. Rutile chemistry and thermometry as provenance indicator: an example from Chios Island, Greece. *Sedimentary Geology,* v. 203, p. 98-111. 2008.

MORTON, A.; CHENERY, S. Detrital rutile geochemistry and thermometry as guides to provenance of Jurassic-Paleocene sandstones of the Norwegian Sea. *Journal of Sedimentary Research*, v. 79, p. 540-553, 2009.

MÜLLER, A.; HALLS, C. Rutile - the tin-tungsten host in the intrusive tourmaline breccia at Wheal Remfry, SW England. In: MAO, J.; BIERLEIN, F. P. *Mineral deposit research:* Berlin-Heidelberg: Springer, 2005. p. 441-444. (*Meeting the global challenge).*

NAVARRO, M. S. *A implantação de rotina e seu refinamento para a determinação de elementos terras raras em materiais geológicos por ICP-OES e ICP-MS:* aplicação ao caso dos granitóides de Piedade-Ibiúna (SP) e Cunhaporanga (PR). 2004. 132 f. Dissertação (Mestrado) - Instituto de Geociências, Universidade de São Paulo, São Paulo, 2004.

PALMER, M. R.; SLACK, J. F. Boron isotopic composition of tourmaline from massive sulfide deposits and tourmalinites. *Contributions to Mineralogy and Petrology*, v. 103, p. 434-451, 1989.

PALMER, M. R.; SWIHART, G. H. Boron isotope geochemistry: An overview. In: GREW, E. S.; ANOVITZ, L. M. (Ed.). *Boron*: mineralogy, petrology and geochemistry. Chantilly, Va: Mineralogical Society of America, 1996. p. 709-744. (*Reviews in Mineralogy,* v. 33).

PEREIRA, R. M. *Caracterização geocronológica, geoquímica, geofísica e metalogênica de alguns plutonitos graníticos da região do médio rio Paraíba do Sul e alto Rio Grande, segmento central da Faixa Ribeira.* 2001. 213 f. Tese (Doutorado) - Universidade Federal do Rio de Janeiro, Rio de Janeiro, 2001.

PEREIRA, R. M.; ÁVILA, C. A.; MOURA, C. A.V. Geologia da região entre Resende e São José do Barreiro e idade $^{207}Pb/^{206}Pb$ do Granito do Funil, segmento central da Faixa Ribeira (RJ-SP), Brasil. *Geociências*, Rio Claro, v. 20, p. 37-48, 2001.

PEREIRA, R. M.; MOURA, C. A. V.; BUSTAMANTE-JUNHO, M. C. Single zircon Pb-evaporation age of some granitic plutons in the central part of the Ribeira Belt, southeastern Brazil. *Revista Brasileira de Geociências*, v. 32, p. 327-334, 2002.

PEREIRA, R. M.; ÁVILA, C. A.; NEUMANN, R. Prospecção para cassiterita na região entre Cachoeira Paulista (SP) e Resende (RJ): potencialidade em estanho dos granitos do Funil e São José do Barreiro, segmento central da Faixa Ribeira. *Geociências*, v. 22, p. 107-119, 2003.

PESQUERA, A.; TORRES-RUIZ, J.; GIL-CRESPO, P. P.; JIANG, S. Y. Petrographic, chemical and B-isotopic insights into the origin of tourmaline-rich rocks and boron recycling in the Martinamor Antiform (Central Iberian Zone, Salamanca, Spain). *Journal of Petrology*, v. 46, p. 1013-1044, 2005.

ROIG, H. L.; DANTAS, E. L.; MENEZES, P. L. Nd isotopes from the Ribeira Belt in the Rio Paraíba do Sul region, SE Brazil: significance for its Neoproterozoic evolution. *Journal of the Virtual Explorer Electronic Edition*, v. 17, Paper 5, p. 1-19, 2004.

SLACK, J. F. Tourmaline associations with hydrothermal ore deposits. In: GREW, E. S. ; ANOVITZ, L. M. (Ed.). *Boron*: mineralogy, petrology and geochemistry. Chantilly, Va: Mineralogical Society of America, 1996. p. 559-644. (Reviews in Mineralogy, v. 33).

SUN, S.; McDONOUGH, W. F. Chemical and isotopic systematics of oceanic basalts: implications for mantle composition and processes. In: SAUNDER, A. D.; NORRY, M. J. (Ed.). *Magmatism in the ocean basins*. Oxford: Blackwell, 1989. p. 313-345. (Geological Society Special Publication, 42).

UFRJ/CPRM. *Geologia da Folha Volta Redonda SF.23-Z-A-V escala 1:100.000*. Rio de Janeiro, Universidade Federal do Rio de Janeiro/Serviço Geológico do Brasil, 2007. 148 p.

WATSON, E. B.; WARK, D. A.; THOMAS, J. B. Crystallization thermometers for zircon and rutile. *Contributions to Mineralogy and Petrology*, v. 151, p. 413-433, 2006.

ZACK, T.; VON EYNATTEN, H.; KRONZ, A. Rutile geochemistry and its potential use in quantitative provenance studies. *Sedimentary Geology*, v. 171, p. 37-58, 2004a.

ZACK, T.; MORAES, R.; KRONZ, A. Temperature dependence of Zr in rutile: empirical calibration of a rutile thermometer. *Contributions to Mineralogy and Petrology*, v. 148, p. 471-488, 2004b.